

IMPROVED ACCURACY IN REGULARIZATION MODELS OF INCOMPRESSIBLE FLOW VIA ADAPTIVE NONLINEAR FILTERING

ABIGAIL L. BOWERS ^{*}, LEO G. REBHOLZ [†], AZIZ TAKHIROV [‡], AND CATALIN
TRENCHEA [§]

Abstract. We study adaptive nonlinear filtering in the Leray regularization model for incompressible, viscous Newtonian flow. The filtering radius is locally adjusted so that resolved flow regions and coherent flow structures are not ‘filtered-out’, which is a common problem with these types of models. A numerical method is proposed that is unconditionally stable with respect to timestep, and decouples the problem so that the filtering becomes linear at each timestep and is decoupled from the system. Several numerical examples are given that demonstrate the effectiveness of the method.

1. Introduction. The Leray- α model of incompressible Newtonian flow is an adaptation of J. Leray’s original Navier-Stokes regularization,

$$v_t + \bar{v} \cdot \nabla v + \nabla p - \nu \Delta v = f \tag{1.1}$$

$$\nabla \cdot v = 0 \tag{1.2}$$

where \bar{v} denotes convolution with a Gaussian with filtering radius $\alpha > 0$ [22]. The only change to (1.1)-(1.2) to get Leray- α is to replace convolution with a Gaussian with the more computationally efficient Helmholtz filter (also called α -filter),

$$-\alpha^2 \Delta \bar{v} + \bar{v} = v. \tag{1.3}$$

Since the Helmholtz filter is an $O(\alpha^4)$ approximation to the Gaussian filter [9], the Leray- α model (1.1)-(1.3) is a high order approximation to Leray’s original model, and the interpretation of α as the filtering radius remains valid. Note that the Navier-Stokes equations (NSE) are recovered when $\alpha = 0$.

The Leray- α model is interesting for many reasons, including its simplicity (in that it ‘looks like’ the NSE, so the NSE tools can be applied), being well-posed [22, 6], conserving energy and 2d enstrophy [6, 27], cascading energy through the inertial range at the same rate as the NSE up to a filtering radius dependent wavenumber [6], then rolling off energy faster than the NSE on subfilter scales which makes it more computable than the NSE [6], and allowing for efficient computations with unconditionally stable linearized algorithms that decouple filtering from the mass/momentum system (in contrast to NS- α , where such algorithms have yet to be discovered [18]). However, attractive theoretical properties do not necessarily produce models that give good results, and unfortunately, the Leray- α model is well-known to over-regularize solutions and even remove critical flow structures [10, 11, 17, 3]. We show herein that by modifying the filter of the Leray- α model to adaptively choose the filtering radius, over-regularization can be avoided and accurate numerical solutions can be obtained. Moreover, when our proposed algorithm is used, i) there is no significant increase in computational cost for the resulting model compared to the usual Leray- α model, ii) stability with respect to timestep is unconditional, and iii) optimal convergence to true physical solutions is achieved. Hence we are able to efficiently obtain accurate solutions with a simple, mathematically sound model.

The filter we consider herein was first proposed in [21], and is based on the phenomenological idea that in laminar regions or where coherent structures persist, little or no filtering

^{*} Department of Mathematical Sciences, Clemson University, Clemson SC 29634, USA. email: abowers@clemson.edu. Partially supported by the NSF under grants DMS-0914478 and DMS-1112593.

[†] Department of Mathematical Sciences, Clemson University, Clemson SC 29634, USA. email: rebholz@clemson.edu. Partially supported by the NSF under grant DMS-0914478 and DMS-1112593.

[‡] Department of Mathematics, University of Pittsburgh, Pittsburgh, PA, 15260, USA. email: azt7@pitt.edu. Partially supported by the NSF under grant DMS-0810385.

[§] Department of Mathematics, University of Pittsburgh, Pittsburgh, PA, 15260, USA. email: trenchea@pitt.edu.

is needed because these regions are resolvable. This is implemented as the nonlinear filter

$$-\alpha^2 \nabla \cdot (a(v) \nabla \bar{v}) + \bar{v} = v, \quad (1.4)$$

where $a(v)$ satisfies, for β some small constant that enforces positivity,

$$\begin{aligned} 0 < \beta < a(v) \leq 1 & \text{ for any fluid velocity } v(x, t), \\ a(v) \simeq 0 & \text{ selects regions requiring no local filtering,} \\ a(v) \simeq 1 & \text{ selects regions requiring } O(\alpha) \text{ local filtering.} \end{aligned}$$

The function $a(u)$ is thus meant to indicate where filtering should be applied, we will refer to it as an *indicator function*. Herein we will study several possible choices of indicator functions, which are presented in Section 2. In [21], this type of nonlinear filtering was used as part of a ‘evolve, then filter, then relax’ approach to evolution equations, and successful numerical results were shown for some small 2D problems. Herein we extend the use of this type of filtering for use with the Leray regularization, and give several 2D and 3D numerical examples to demonstrate its effectiveness.

In the periodic setting, the well-posedness of (1.1)-(1.2)-(1.3) is guaranteed by $\alpha > 0$, and similarly well-posedness can be shown for (1.1)-(1.2)-(1.4) when $\beta > 0$. Outside of the periodic case, care must be taken with the formulation to retain a well-posed system. Specifically, standard energy estimates require $\nabla \cdot \bar{v} = 0$ [31], which is not equivalent to (1.2) outside of the periodic case, and so it must be enforced. But given a v , the filters discussed above are linear and positive, and so have unique solutions; thus enforcing a solenoidal constraint on \bar{v} overdetermines the system. The fix is to add a Lagrange multiplier to the filter, and then enforce solenoidal constraints on both v and \bar{v} , resulting in the following system:

$$v_t + \bar{v} \cdot \nabla v + \nabla p - \nu \Delta v = f \quad (1.5)$$

$$\nabla \cdot v = 0 \quad (1.6)$$

$$-\alpha^2 \nabla \cdot (a(v) \nabla \bar{v}) + \bar{v} + \nabla \lambda = v \quad (1.7)$$

$$\nabla \cdot \bar{v} = 0 \quad (1.8)$$

REMARK 1.1. *The solution v of this model can still be interpreted as an averaged velocity, although in a slightly different sense than usual since the averaging radius is chosen locally by $\sqrt{a(v(x))}\alpha$.*

We will present a numerical algorithm for the system (1.5)-(1.8) that decouples the conservation system (1.5)-(1.6) from the incompressible filter system (1.7)-(1.8), and provides an efficiently computable well-posed discrete system.

We note this is not the first attempt at modifying the regularization in Leray- α and related models in order to improve accuracy. To our knowledge, the best attempt has been the addition of van Cittert approximate deconvolution to the filter. This has been found successful in Leray- α , NS- α , and NS- $\bar{\omega}$ models [3, 17, 18, 28, 20]. However, there are two drawbacks to this technique not present in the proposed method. First, the gain in accuracy from using deconvolution requires the use of higher order elements, which can be more expensive to implement, provide less freedom in meshing, and make it computationally infeasible to ‘crank out one more mesh.’ Second, the accuracy near the boundary remains an open question; that is, on no-slip boundaries, we are not sure that error goes to zero as α and the meshwidth tends to zero [3, 18].

This paper is arranged as follows. Section 2 contains preliminaries, introduces the indicator functions, presents a numerical method for (1.5)-(1.8), and discusses stability and convergence of the method. Section 3 presents the results of four numerical experiments, each of which demonstrating that the model/method is very effective at finding accurate solutions on coarse meshes, and is much more accurate than the usual Leray- α model.

2. Nonlinear adaptive filtering in the Leray model. In this section, we precisely define the finite element algorithms to discretize the models discussed above. To begin, we present some mathematical preliminaries. Then we define the discrete filter and the associated indicator functions we will use. Finally, we present the scheme for the Leray model, and provide stability and convergence results.

2.1. Preliminaries. We denote by Ω an open, simply connected domain with piecewise smooth boundary. The $L^2(\Omega)$ norm and inner product will be denoted by $\|\cdot\|$ and (\cdot, \cdot) . For simplicity of the presentation, we assume no-slip boundary conditions, but extension to other Dirichlet, Neumann or Robin boundary conditions would be done in the usual way. In this setting, the appropriate velocity and pressure spaces are defined as

$$X := (H_0^1(\Omega))^d, \quad Q := L_0^2(\Omega).$$

We use as the norm on X , $\|v\|_X := \|\nabla v\|_{L^2}$, and denote the dual space of X by X^* , with the norm $\|\cdot\|_*$. The space of divergence free functions is given by

$$V := \{v \in X : (\nabla \cdot v, q) = 0 \quad \forall q \in Q\}.$$

We denote conforming velocity, pressure finite element spaces based on an edge to edge triangulations (tetrahedralizations) of Ω (with maximum element diameter h) by

$$X_h \subset X, \quad Q_h \subset Q.$$

We assume that X_h, Q_h satisfy the usual inf-sup stability condition [12]. For our computations, we use Taylor-Hood and Scott-Vogelius element pairs (in the appropriate setting), both of which are known to satisfy the inf-sup condition [4, 33, 1].

2.2. Discrete Filtering. Given an indicator function $a(\cdot)$, a fluid velocity $u \in X$, an averaging radius α (possibly varying with x), we define the filtered velocity \bar{u}^h using a selected indicator function, $a(\cdot)$, as the solution of: Find $(\bar{u}^h, \lambda_h) \in X_h \times Q_h$ satisfying

$$\alpha^2(a(u)\nabla\bar{u}^h, \nabla v_h) + (\bar{u}^h, v_h) - (\lambda_h, \nabla \cdot v_h) = (u, v_h) \quad \forall v_h \in X_h, \quad (2.1)$$

$$(\nabla \cdot \bar{u}^h, q) = 0 \quad \forall q \in Q_h. \quad (2.2)$$

As discussed in the introduction for the continuous case, the Lagrange multiplier term λ_h allows the solenoidal constraint to be enforced. Note that if the chosen element pair is used whose weak enforcement of mass conservation does not provide ‘good’ mass conservation, e.g. Taylor-Hood elements [5], then grad-div stabilization should be added to (2.1) to improve mass conservation and overall accuracy [16]. Consideration of mass conservation is particularly important in regularization models, where coarse meshes are used, and thus relying on global mass conservation may not be sufficient to provide physically relevant solutions.

When $u \in X$ is given input for the filter system (2.1)-(2.2), nonlinear filtering is made a linear problem. It is shown in [21] that solutions exist uniquely, and satisfy

$$2 \int_{\Omega} \alpha^2 a(u) |\nabla \bar{u}^h|^2 dx + \|\bar{u}^h\|^2 \leq \|u\|^2. \quad (2.3)$$

Error in discrete filtering is also considered in [21] and the following result is proven, which shows what is lost through this discrete filtering is due only to discretization error and the filtering radius.

THEOREM 2.1. *Consider the discrete nonlinear filter \bar{u}^h given by (2.1), with $u \in V$. We have*

$$\begin{aligned} & \int_{\Omega} \alpha^2 a(u) |\nabla(u - \bar{u}^h)|^2 dx + \|u - \bar{u}^h\|^2 \\ & \leq C \inf_{\tilde{u} \in X_h} \left\{ \int_{\Omega} \alpha^2 a(u) |\nabla(u - \tilde{u})|^2 dx + \|u - \tilde{u}\|^2 \right\} + C\alpha^4 \|\nabla \cdot (a(u)\nabla u)\|^2. \end{aligned}$$

A similar result for $u \in X$ can be proven [21].

2.2.1. Indicator functions. We consider the following indicator functions, for use with the filter (2.1)-(2.2).

1. The Q-criterion based indicator

The most popular method for eduction of coherent vortices is the Q criterion, which was developed in [13], and is defined as follows. Define deformation and spin tensors by

$$\nabla^s u := \frac{1}{2} (\nabla u + \nabla u^{tr}) \quad \text{and} \quad \nabla^{ss} u := \frac{1}{2} (\nabla u - \nabla u^{tr}).$$

A persistent and coherent vortex is found at regions where spin (local rigid body rotation) dominates deformation, i.e. where

$$Q(u, u) := \frac{1}{2} (\nabla^{ss} u : \nabla^{ss} u - \nabla^s u : \nabla^s u) > 0.$$

It is a necessary condition (in 3d) and both necessary and sufficient (in 2d) for slower than exponential local separation of trajectories.

We define a Q-criterion based indicator function so that $Q(u, u) > 0$ implies $a(u) \simeq 0$ (we note there are many ways to do this, and this way is certainly improvable), and is given by

$$a_Q(u) := \frac{1}{2} - \frac{1}{\pi} \arctan \left(\alpha^{-1} \frac{Q(u, u)}{|Q(u, u)| + \alpha^2} \right).$$

2. Vreman's eddy viscosity based indicator

In [32], using only the gradient tensor, Vreman constructs an eddy viscosity coefficient formula that vanishes identically for 320 types of flow structures that are known to be coherent (non turbulent). Define

$$|\nabla u|_F^2 = \sum_{i,j=1,2,3} \left(\frac{\partial u_j}{\partial x_i} \right)^2, \beta_{ij} := \sum_{m=1,2,3} \frac{\partial u_i}{\partial x_m} \frac{\partial u_j}{\partial x_m}, \text{ and}$$

$$B(u) := \beta_{11}\beta_{22} - \beta_{12}^2 + \beta_{11}\beta_{33} - \beta_{13}^2 + \beta_{22}\beta_{33} - \beta_{23}^2.$$

Then

$$\text{Vreman's eddy viscosity coefficient} = C\alpha^2 \left\{ \begin{array}{l} \sqrt{\frac{B(u)}{|\nabla u|_F^4}}, \text{ if } |\nabla u|_F \neq 0 \\ 0, \text{ if } |\nabla u|_F = 0, \end{array} \right\}$$

where C is a positive tuning constant. Since $0 \leq B(u)/|\nabla u|_F^4 \leq 1$ we take as an indicator function,

$$a_V(u) = \sqrt{\frac{B(u)}{|\nabla u|_F^4}}.$$

3. Relative helicity-based indicator

The relative helicity density is the helicity density scaled by the magnitude of velocity and vorticity. Helicity $H(t)$, helicity density $HD(x, t)$ and relative helicity density $RH(x, t)$ are given respectively as follows

$$H(t) := \frac{1}{|\Omega|} \int_{\Omega} u \cdot (\nabla \times u) dx,$$

$$HD(x, t) := \frac{1}{|\Omega|} u(x, t) \cdot (\nabla \times u(x, t)), \text{ and}$$

$$RH(x, t) := \frac{u(x, t) \cdot \omega(x, t)}{|u(x, t)| |\nabla \times u(x, t)|}.$$

If the NSE nonlinearity is in rotational form, the helicity, $u \cdot \omega$, and the NSE nonlinearity, $u \times \omega$, are related by

$$\frac{\text{Helicity}^2 + |\text{NSE nonlinearity}|^2}{|u|^2|\omega|^2} = 1.$$

Thus (local) high helicity suppresses (local) turbulent dissipation caused by breakdown of eddies into smaller ones by the NSE nonlinearity. For example, storm cells (with low helicity) break down rapidly due to nonlinear interactions while rotating “supercell” thunderstorms (with high helicity) maintain their structure over much longer time scales [25]. Different rates of eddy breakdown due to (local) high or low helicity has even been taken to explain intermittence, Levich and Tsouber [24], [23], [30], Betchov [2]. Thus we develop an indicator function by adjusting relative helicity density so the values near one imply $a(u) \simeq 0$ so that $u \simeq \bar{u}$. Among the many possible ways to do this, we propose the following.

$$a_H(u) := 1 - \left| \frac{u(x, t) \cdot \omega(x, t)}{|u(x, t)||\omega(x, t)| + \delta^2} \right|.$$

4. Synthesized methods

Given indicator functions a_i , constructing synthesized indicator functions can be easily done via

$$a_{ij}(u) := (a_i(u)a_j(u))^{1/2}. \quad (2.4)$$

With this method, combining two indicator functions that have different selection criteria can produce a better indicator. In our numerical experiments, the best results are usually obtained with a synthesized indicator.

2.3. Numerical algorithm for Leray model. We propose the following finite element algorithm to compute solutions to the Leray regularization model with adaptive nonlinear filtering.

ALGORITHM 2.2. *Given a forcing $f \in L^\infty(0, T; H^{-1}(\Omega))$, an initial velocity $u_0 \in V$, a timestep $\Delta t > 0$, endtime T and integer M satisfying $T = M\Delta t$, define $u_h^{-1} = u_h^0$ to be the L^2 projection into V_h of u_0 . Then for a fixed constant α chosen of the order of the mesh width, and given indicator function $0 \leq a(\cdot) \leq 1$, find $(u_h^n, p_h^n) \in (X_h, Q_h)$, $n = 1, 2, \dots, M$ satisfying*

$$\begin{aligned} \frac{1}{\Delta t}(v_h^{n+1} - v_h^n, \chi_h) + \left(\frac{3}{2}v_h^n - \frac{1}{2}v_h^{n-1} \cdot \nabla v_h^{n+\frac{1}{2}}, \chi_h \right) \\ - (p_h^{n+1/2}, \nabla \cdot \chi_h) + \nu(\nabla v_h^{n+\frac{1}{2}}, \nabla \chi_h) = (f(t^{n+\frac{1}{2}}), \chi_h) \quad \forall \chi_h \in X_h, \quad (2.5) \\ (\nabla \cdot v_h^{n+1}, q_h) = 0 \quad \forall q_h \in Q_h \quad (2.6) \end{aligned}$$

REMARK 2.3. *An initial pressure is not needed, provided the first step is taken using a backward Euler type temporal discretization.*

REMARK 2.4. *If a choice of (X_h, Q_h) is used that does not provide pointwise divergence-free solutions to the filtering problem (e.g. Taylor-Hood), then the nonlinear term in (2.5) should be skew-symmetrized as in [17], and grad-div stabilization should also be added to (2.5).*

There are several important properties of this discretization. By using a Crank-Nicolson temporal discretization and linear extrapolation of the filtered term, formal second order temporal accuracy is retained while decoupling the filter from the conservation law system and linearizing filter computations; hence at each timestep, two linear solves are needed. In the discrete filter solve (2.1)-(2.2), the u will be known, and so the filtering will be linear(!)

and the extra cost is in the calculation of $a(u)$ (which is negligible for our chosen indicator functions), and also in updating a preconditioner after so many timesteps, depending on the solver method being employed. Moreover, this scheme is unconditionally stable with respect to timestep, as stated in the next lemma. We note these important algorithmic properties (or analogs of them) also hold if a linearized BDF2 is used instead of Crank-Nicolson See, for example, [8, 19].

LEMMA 2.5. *For any choice of time step $\Delta t > 0$, solutions to Algorithm 2.2 satisfy*

$$\|v_h^M\|^2 + \nu \Delta t \sum_{n=0}^{M-1} \|\nabla v_h^{n+1/2}\|^2 \leq C(\text{data}). \quad (2.7)$$

Proof. Choose $\chi_h = v_h^{n+1/2}$. The nonlinear term(s) vanishes, due to skew symmetrization or directly, if the filtered extrapolated velocity is pointwise divergence-free. The pressure term vanishes since we can choose $q_h = p_h^{n+1}$ in (2.6). This leaves

$$\frac{1}{2\Delta t} (\|v_h^{n+1}\|^2 - \|v_h^n\|^2) + \nu \|\nabla v_h^{n+1/2}\|^2 = (f(t^{n+\frac{1}{2}}), v_h^{n+\frac{1}{2}}).$$

Applying Cauchy-Schwarz and Young's inequalities to the right-hand side, multiplying through by Δt , summing over time steps, and using the smoothness assumptions on the problem data gives the result. \square

REMARK 2.6. *Since the filter system is linear (in the unknown) and stable, the result (5) is sufficient to show that Algorithm 2.2 is well-posed. A proof of well-posedness is included in the Appendix.*

For simplicity in stating the following convergence theorem, we summarize here the necessary regularity assumptions for the solution $(u(x, t), p(x, t))$ to the NSE

$$u \in L^\infty(0, T; H^{k+1}(\Omega) \cap H^3(\Omega)), \quad (2.8)$$

$$p \in L^\infty(0, T; H^k(\Omega)), \quad (2.9)$$

$$\Delta u_{tt}, u_{ttt} \in L^2(0, T; L^2(\Omega)). \quad (2.10)$$

Since the adaptive filter differs from the α -filter only by the indicator function which satisfies $0 < a(\cdot) \leq q$, solutions from Algorithm 2.2 must have consistency to the NSE at least as good as Leray- α solutions (i.e. when $a(\cdot) = 1$). We have the following convergence result for the algorithm:

THEOREM 2.7. *Let $(u, p) \in (V, Q)$ be a strong NSE solution on $\Omega \times (0, T]$ for a given set of data f , u_0 , ν , satisfying (2.8)-(2.10). Then if (u_n, p_n) , $n = 0, 1, \dots, M$ is the solution to Algorithm 2.2 using (P_k, P_{k-1}^{disc}) Scott-Vogelius elements, and for $\Delta t > 0$, the velocity error satisfies*

$$\|u(T) - u_h^M\|^2 + \nu \Delta t \sum_{n=0}^{M-1} \|\nabla(u(t^{n+1/2}) - u_h^{n+1/2})\|^2 \leq C_u (\Delta t^4 + h^{2k} + \alpha^4), \quad (2.11)$$

and the pressure error satisfies

$$\begin{aligned} \Delta t \sum_{n=0}^{M-1} \|p_h^{n+1/2} - p(t_{n+1/2})\|^2 &\leq C_{p_1} ((\Delta t)^4 + \alpha^2 h^{2k} + h^{\min\{2k+2, 2s\}}) \\ &+ C_{p_2} (h^{-1}((\Delta t)^4 + \alpha^4 + h^{2k}) + h^{-3}((\Delta t)^8 + \alpha^8 + h^{4k})) \end{aligned} \quad (2.12)$$

where C_u , C_{p_1} , and C_{p_2} are constants dependent on data and the true solution.

Proof. The proofs are given in the appendix. \square

3. Numerical Experiments. In this section, we present several numerical experiments that illustrate the effectiveness of our proposed approach, in giving good coarse mesh approximations of incompressible flows. In particular, we will show this approach gives much better results than for the usual Leray- α model, and gives good approximations on meshes where the NSE is significantly underresolved when computed directly. We note that the extra cost of using the indicator function (versus $a(v) = 1$ in the case of Leray- α) was negligible in our computations. This is due to the chosen timestepping algorithm, which decouples the filtering and momentum solves, but also linearizes the filter, making the only extra cost the calculation of $a(v)$ for a given v .

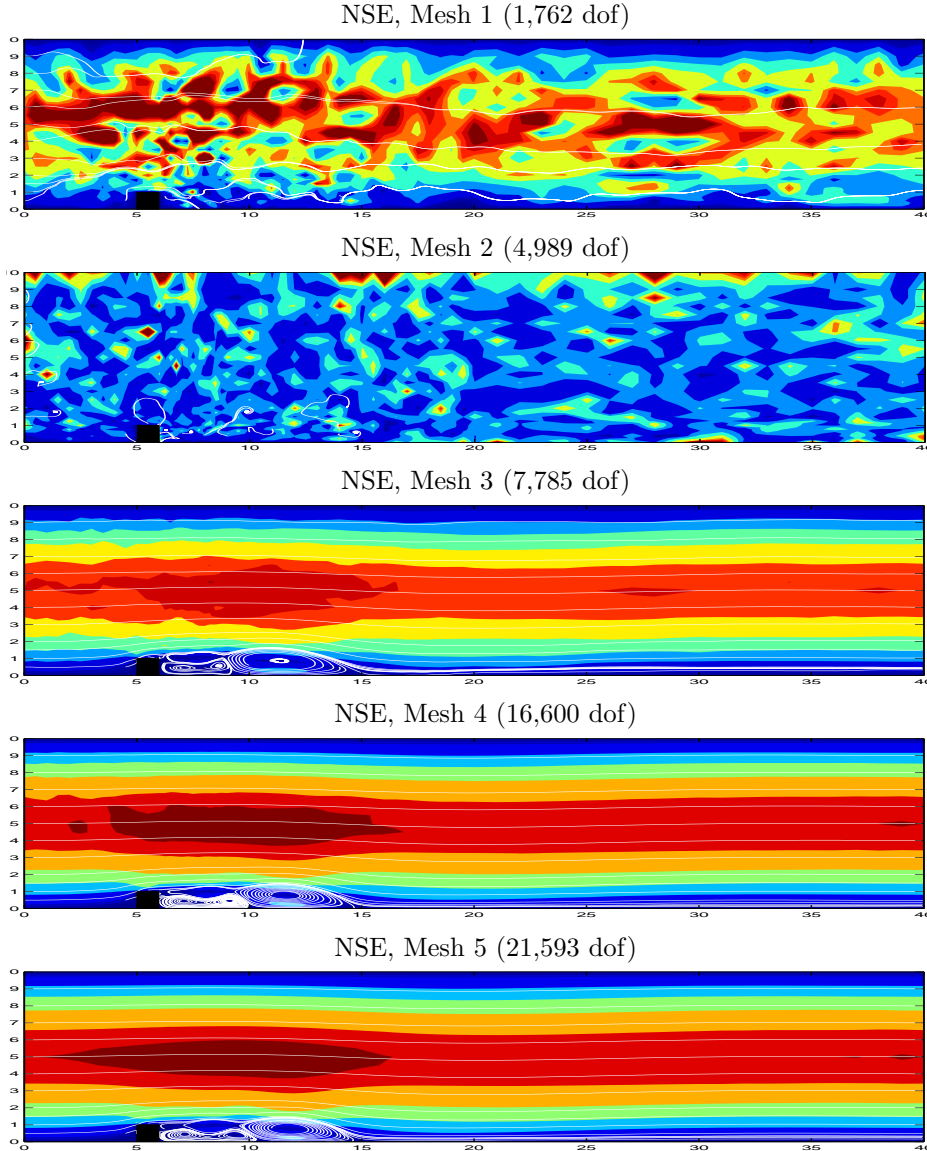


FIG. 3.1. Shown above is the velocity solutions at $T = 40$ for 2D flow over a step, found by directly computing the Navier-Stokes equations (i.e. no filtering), on different meshes. Only the finest mesh correctly predicts the true solution.

3.1. 2D channel flow over a step. Our first experiment is for two-dimensional flow over a forward and backward facing step. The domain is a 40 x 10 rectangular channel with a 1 x 1 step five units into the channel at the bottom. We assume no-slip boundary conditions

on the top and bottom boundaries, a parabolic inflow profile given by $(y(10 - y)/25, 0)^T$, and a zero-traction (do-nothing) outflow. The correct behavior is a smooth velocity field away from the step, and for eddies to periodically form and shed behind the step.

We first present the results of computing the NSE directly. Computations were made on five successively finer meshes, using $\Delta t = 0.01$ and $\nu = 1/600$, and Taylor-Hood elements. Solutions at $T = 40$ are shown in Figure 3.1 as velocity streamlines over speed contours, and we observe only the finest mesh gets the correct solution, comparing to [17]. The solution is very under-resolved on the coarsest two meshes, and on meshes 3 and 4, the predicted solution captures the eddy formation and detachment, but oscillations are still observed in the speed contours.

We test the proposed model with Algorithm 2.2 on the two coarsest meshes, using the same parameters as for the coarse mesh NSE computation, and using indicator functions $a(u) = 1$, a_V , a_Q , and a_{VQ} . Results for Mesh 2 (which provides 4,989 dof) at $T = 40$ are shown in Figure 3.2. All four filters found a smooth flow field, but the Vreman filter and VQ-filter also capture the correct eddy detachment behind the step. Contour Plots of the different indicator functions at $T = 40$ are shown for these computations in Figure 3.3. For this example, we see the V and VQ have expected behavior in that little or no filtering is required away from the step. These two indicators suggest filtering is needed near the center of the channel, and we believe this to be a result of the laminar profiles predicted by NSE and regularization models to be slightly different [3], and so a mixing of the two could cause numerical artifacts. The Q indicator plot is quite different. It finds near the step areas to filter and not to filter, which is expected, but throughout the rest of the channel it gives values near 0.5. From the definition of our filter, the values near 0.5 correspond to $Q(u, u) = 0$, and so this suggests additional tuning of a_Q could be helpful (for this particular problem). We also present a plot of the velocity solution obtained using the VQ-filter on Mesh 1, in Figure 3.4. Here, with only 1,762 dof, a good approximation that predicts eddy detachment is found.

3.2. 2D Flow around a cylinder. Our next numerical experiment is for two dimensional under-resolved channel flow around a cylinder, a well known benchmark problem taken from Schäfer and Turek [29] and John [14]. The flow patterns are driven by the interaction of a fluid with a wall which is an important scenario for many industrial flows. This simple flow is actually quite difficult to simulate successfully by a model with sufficient regularization to handle higher Reynolds number problems.

The domain for the problem is a 2.2×0.41 rectangular channel with a cylinder of radius 0.05 centered at $(0.2, 0.2)$ (taking the bottom left corner of the rectangle as the origin). The cylinder, top and bottom of the channel are prescribed no slip boundary conditions, and the time dependent inflow and outflow profile are

$$\begin{aligned} u_1(0, y, t) = u_1(2.2, y, t) &= \frac{6}{0.41^2} \sin(\pi t/8) y(0.41 - y), \\ u_2(0, y, t) = u_2(2.2, y, t) &= 0. \end{aligned}$$

The viscosity is set as $\nu = 10^{-3}$ and the external force $f = 0$. From time $t = 2$ to $t = 4$, the correct behavior is for two vortices start to develop behind the cylinder. They then separate into the flow, and soon after a vortex street forms which can be visible through the final time $t = 8$. A plot of the resolved $t = 6$ solution is shown in Figure 3.5.

We compute solutions to Algorithm 2.2 with Taylor-Hood elements on a triangular mesh providing 14,446 total degrees of freedom, with time step $\Delta t = 0.001$, and filtering radius α chosen to be the average mesh width, with varying indicator functions. These simulations are all under-resolved; fully resolved computations of the Navier-Stokes equations use upwards of 100,000 degrees of freedom and even smaller time steps. Thus we do not expect exact agreement with solutions of Algorithm 2.2 with the true solution or lift and drag reference values. However, we do expect answers to be close, if this model/algorithm is to be considered useful.

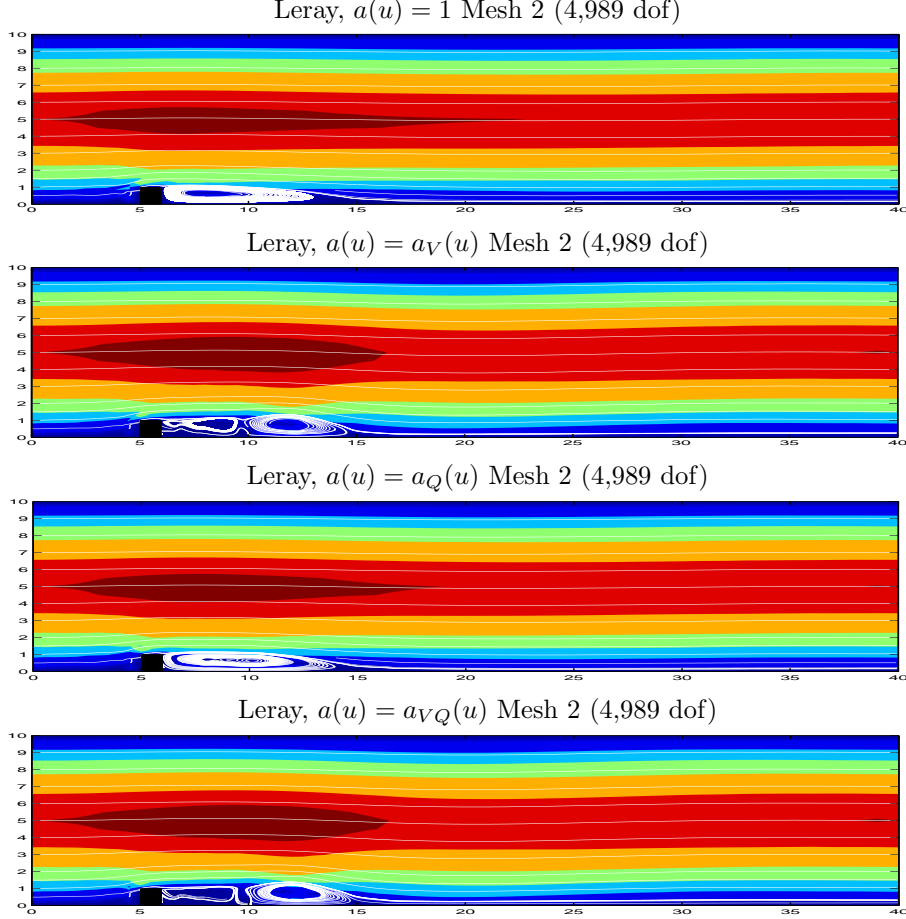


FIG. 3.2. Shown above are the velocity solutions for $T = 40$ for 2D flow over a step, for the Leray model with the usual Leray- α model (top) and several choices of indicator functions, on mesh level 1.

To evaluate the solutions, we compute values for the maximal drag $c_{d,max}$ and lift $c_{l,max}$ coefficients at the cylinder, and for the pressure difference $\Delta p(t)$ between the front and back of the cylinder at the final time $T = 8$. Lift and drag coefficients (using the one dimensional method described by V. John [14]) for fully resolved flows will lie in the reference intervals ([29])

$$c_{d,max}^{ref} \in [2.93, 2.97], \quad c_{l,max}^{ref} \in [0.47, 0.49], \quad \Delta p^{ref} \in [-0.115, -0.105]$$

We test Algorithm 2.2 with indicator functions $a(u) = 1$, a_V , a_Q , and a_{VQ} . The maximum lift and drag coefficients and pressure drop for the simulations are given in Table 3.1, and we see that our algorithm performs well with all three nonlinear filters, but is much less accurate when the linear filter is used. Even on a finer mesh with 56,477 the linear filter (i.e. usual α -filter) still does not perform as well as the nonlinear filters on the coarser mesh (Table 3.1).

3.3. 3D channel flow around a ‘square cylinder’. Our next experiment is for 3D channel flow around a square cylinder, following the setup described in [29]. The channel is modeled as a $0.41 \times 2.5 \times 0.41$ rectangular box, with a $0.41 \times 0.1 \times 0.1$ block placed in the channel (and attached to the side walls) as in Figure 3.6. We compute for $0 \leq t \leq 8 = T$,

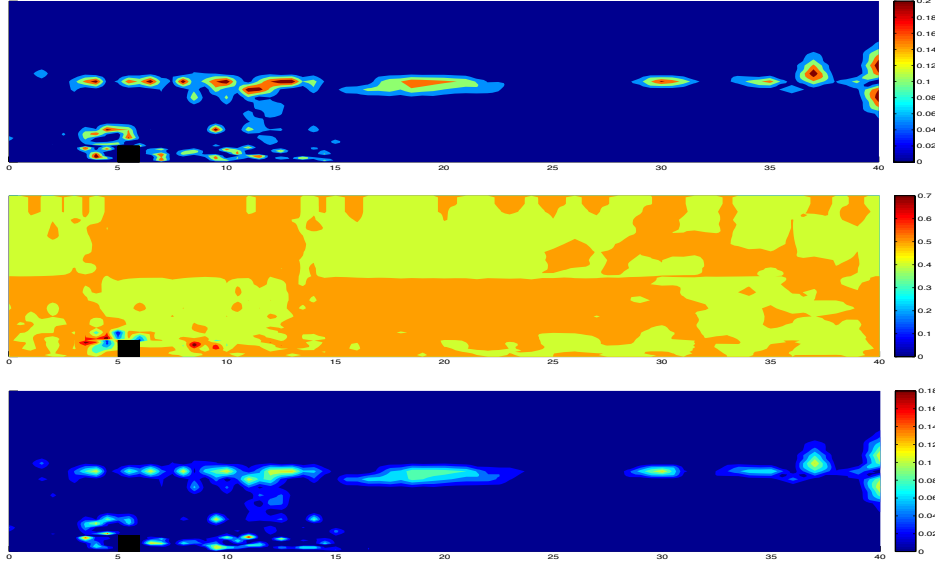


FIG. 3.3. Contour plots of the Vreman Filter (top), Q-Filter (middle) and VQ-Filter (bottom), mesh 1, $T = 40$.

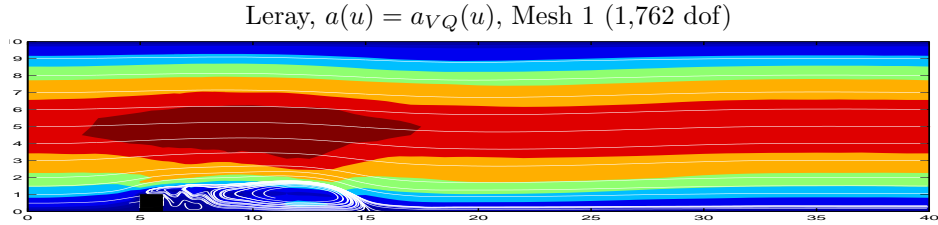


FIG. 3.4. Shown above are the velocity solutions at $T = 40$ for 2D flow over a step, for the Leray model with the VQ indicator function, on mesh level 1.

Indicator	dof	$c_{d,max}$	$c_{l,max}$	Δp
$a(u) = 1$	14,446	2.2844	0.0176	-0.1267
$a_V(u)$	14,446	2.8472	0.4010	-0.1138
$a_Q(u)$	14,446	2.8574	0.4019	-0.1134
$a_{VQ}(u)$	14,446	2.8628	0.4051	-0.1135
$a(u) = 1$	56,477	2.6682	0.2879	-0.1067
DNS Reference Values	>100,000	[2.93,2.97]	[0.47,0.49]	[-0.115,-0.105]

TABLE 3.1

Lift, drag and pressure drop for the flow around a cylinder experiment with varying indicator functions used in the filtering.

using $\nu = 0.001$, the inflow condition is given by

$$u(0, y, t) = \begin{pmatrix} 0 \\ 4(1.5)y(0.41 - y)/(0.41^2) \sin(\pi t/8) \\ 0 \end{pmatrix},$$

we use no-slip boundary conditions on the cylinder as well as the walls of the channel, enforce an appropriate outflow boundary condition, and take the initial condition to be $u_0 = 0$. We compute with the indicator functions $a(u) = 1$ (usual Leray- α model), $a_Q(u)$, $a_V(u)$, $a_{VQ}(u)$, and $a_H(u)$, using the fixed timestep $\Delta t = 0.01$. $((P_3)^3, P_2^{disc})$ Scott-Vogelius elements are used on a barycenter refinement of a coarse tetrahedral mesh (and thus are

Resolved NSE solution at t=6

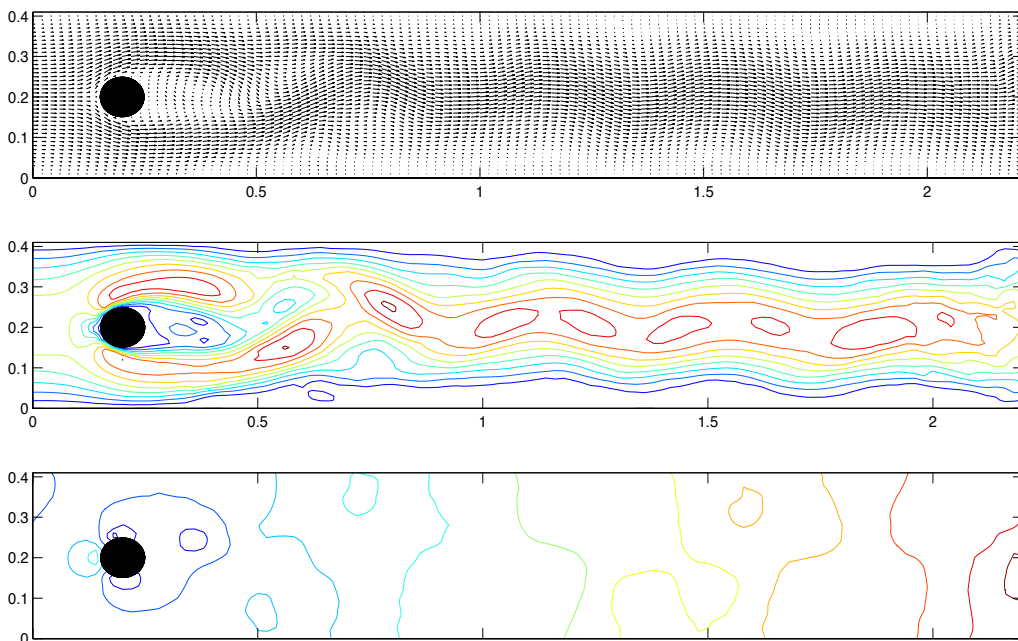


FIG. 3.5. Shown above are the (top) velocity field, (middle) speed contours, and (bottom) pressure contours for the resolved $t = 6$ solution to the 2D channel flow around a cylinder problem.

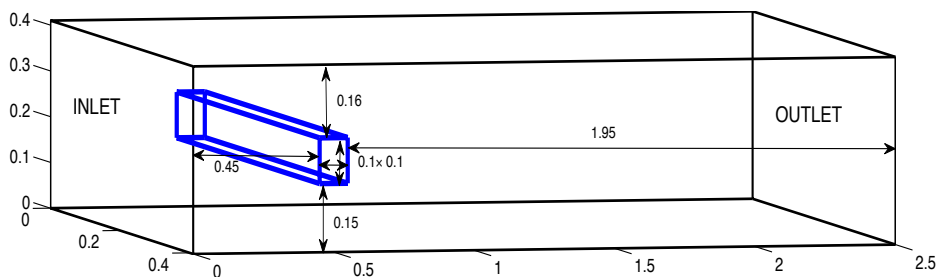


FIG. 3.6. Shown above is the domain for the 3D channel flow over a step problem.

LBB stable [33]), via the method developed in [26], yielding 246,726 total degrees of freedom. Lift and drag coefficients (c_d, c_l) are computed at each timestep via global integrals (see [14]), and maximum values of the coefficients are given in Table 3.2. Comparing to the reference values given in [29]: [4.3, 4.5] for $c_{d,max}$, and [0.01,0.05] for $c_{l,max}$, which were determined based on several direct numerical simulations using upward of six million total degrees of freedom, we observe that the adaptive filtering with the VQ-based indicator function is the only one to predict maximum lift to within the reference value tolerance, and both Q-based and VQ-based indicator functions are close to finding the maximum drag coefficient to within the specified tolerance.

For further comparison of the methods' solutions, we plot them below as streamlines over speed contours at the mid-sliceplanes when $t = 5$. Figure 3.7 shows a resolved solution resulting from directly computing the NSE on a finer mesh that yields over 1.1 million degrees of freedom; we will use this plot as a reference comparison for the regularized

Filter	dof	$c_{d,max}$	$c_{l,max}$
$a(u) = 1$	246,726	2.7536	0.0023
$a(u) = a_V(u)$	246,726	3.510	0.0020
$a(u) = a_Q(u)$	246,726	4.2731	0.0039
$a(u) = a_{VQ}(u)$	246,726	4.0337	0.0185
$a(u) = a_H(u)$	246,726	2.8131	0.0017
DNS Reference Values	> 6,000,000	[4.3, 4.5]	[0.01,0.05]

TABLE 3.2

Maximum lift and drag coefficients for the 3D flow around a cylinder experiment with different indicator function filters.

solutions. This figure also shows the usual Leray- α solution, and we observe the predicted wake has a much different character compared to the resolved NSE solution, and displays the over-regularized behavior commonly known to happen with this model. Solutions from the Leray-regularization with different indicator functions are shown in Figure 3.8. The solutions from the VQ-based and Q-based indicator function regularizations both capture the general behavior of the resolved NSE solution. The Vreman-based indicator function solutions shows some improvement over the usual Leray- α solution. A plot of the helicity-based indicator function solution is omitted, as it looks identical to the usual Leray- α solutions (i.e. there was no visible improvement from using a_H).

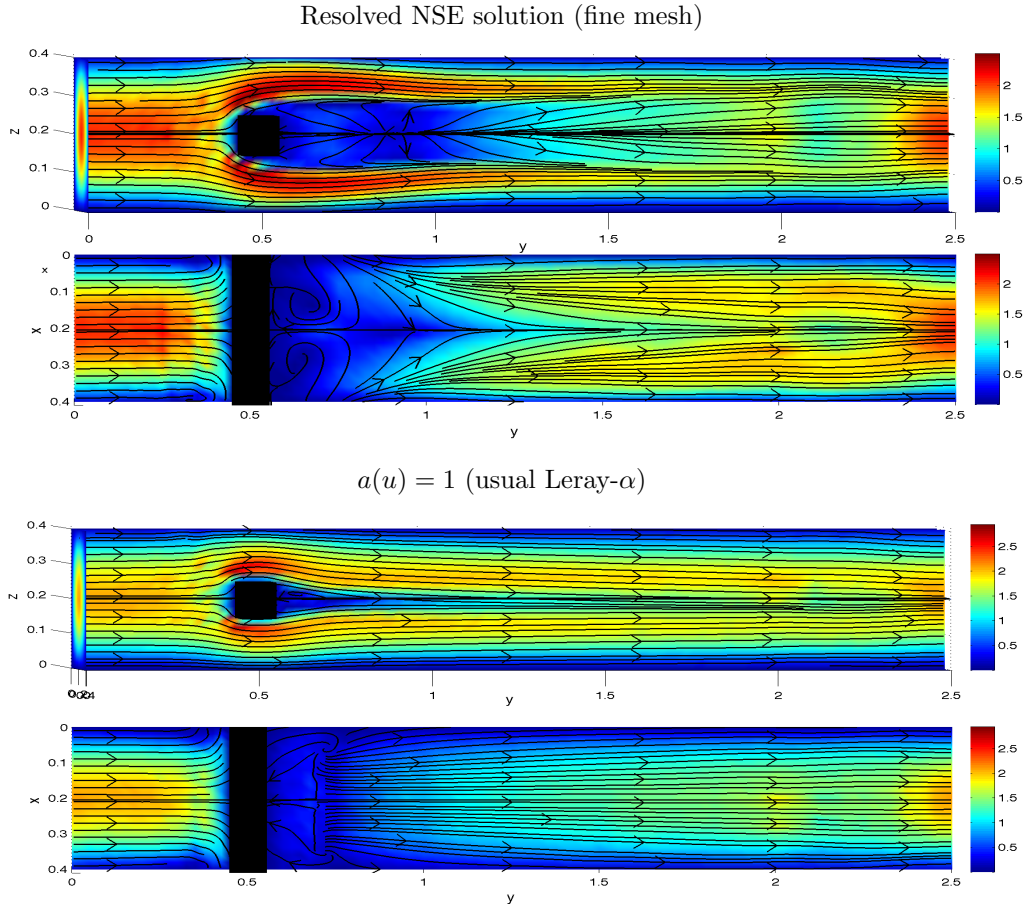


FIG. 3.7. Shown above is velocity streamlines and speed contours on the mid-sliceplanes of the $t = 5$ velocity solutions for 3D flow over a square cylinder, on a fine mesh as a direct computation with the NSE (top), and for the usual Leray- α model on the coarse mesh.

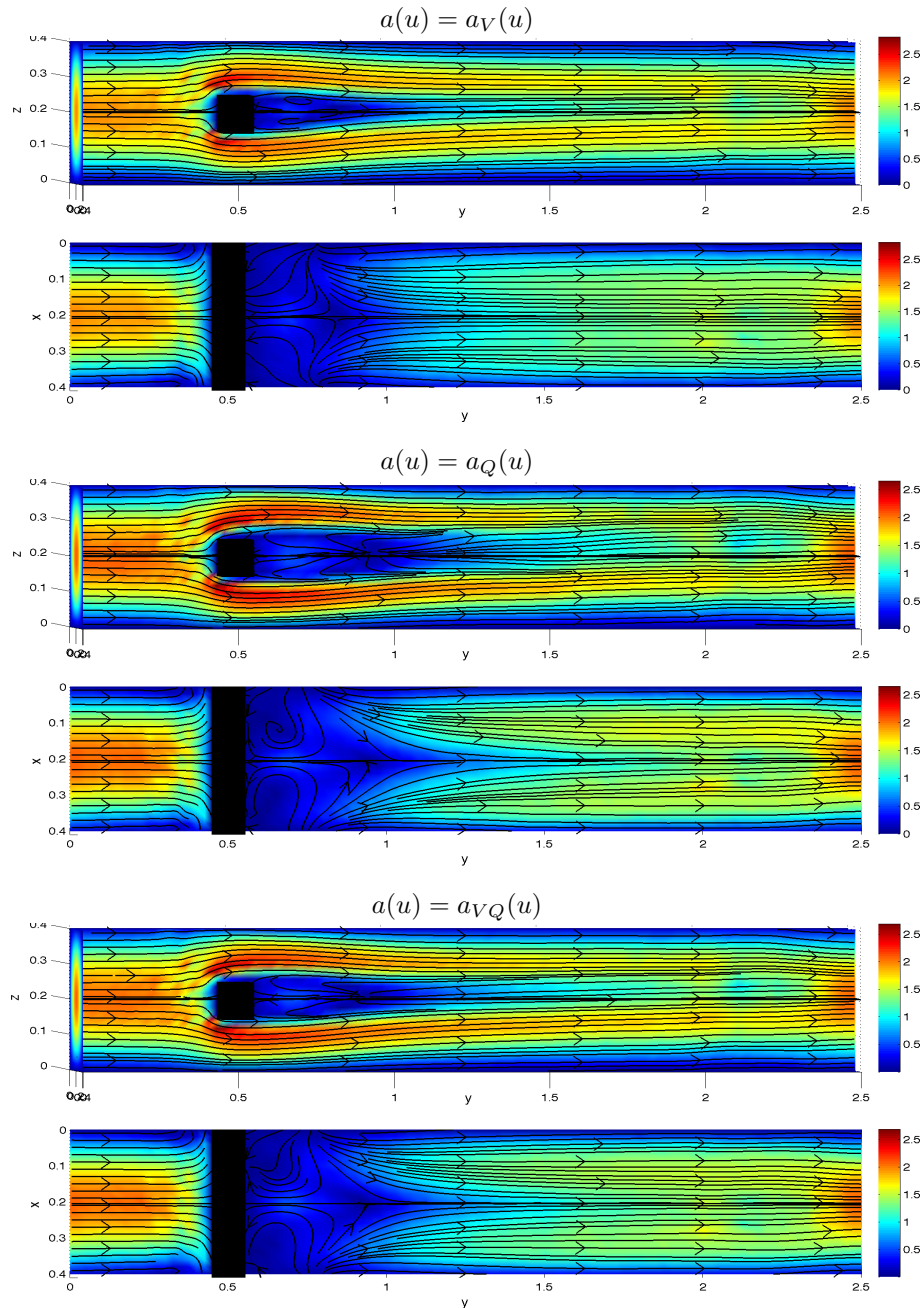


FIG. 3.8. Shown above is velocity streamlines and speed contours on the mid-sliceplanes of the $t = 6$ velocity solutions for 3D flow over a square cylinder, for the Leray model with several choices of indicator functions, on a coarse mesh.

3.4. 3D channel flow over a forward-backward step. Our final numerical test is for time dependent 3D channel flow over a forward-backward facing step with $Re = 200$. This problem is a 3D analog of the 2D step problem presented above, and a diagram of the flow domain is given in Figure 3.9; the channel is $10 \times 40 \times 10$ with a $10 \times 1 \times 1$ block on the bottom of the channel, 5 units in from the inlet. No slip boundary conditions are enforced on the channel walls and on the step. An inflow=outflow condition is enforced, and the initial condition is the solution of the $Re = 50$ steady flow. We compute with $((P_3)^3, P_2^{disc})$ Scott-Vogelius elements on a barycenter refined tetrahedralization of the domain, via the



FIG. 3.9. Shown above is domain for the 3D channel flow over a step problem.

method of [26], and a uniform timestep of $\Delta = 0.025$ is used to compute solutions up to end-time $T = 10$. This flow was studied in [7], and the correct behavior at $T = 10$ is for an eddy to have detached from behind the step and moved down the channel, and a new eddy to form. For the direct numerical simulation of this problem that was performed in [7], the total spatial degrees of freedom needed to resolve this flow was 1,282,920. We test our methods on a much coarser mesh that gives 193,596 total degrees of freedom.

Plots of the solutions obtained by the methods for indicator functions $a(u) = 1$ (usual Leray- α), a_H , a_Q , a_V , and a_{VQ} , are shown in Figure 3.10. Neither the usual Leray- α model nor the filter with helicity indicator function are able to predict eddy detachment. However, the methods using filters with Q-criterion based, Vreman-based, and VQ synthesized indicator functions all predict eddy detachment. Of the three, the VQ-based filter appears to resolve it best; a zoomed in look at the streamribbons near the step in Figure 3.11 shows a more refined picture of its eddy separation, and matches the solution of [7] qualitatively well.

4. Conclusions. We proposed an unconditionally stable and efficient algorithm for computing reduced order approximations to flow problems, by using adaptive nonlinear filtering with the Leray regularization model. We have found this method to be very effective, and to give much better solutions on coarse meshes than either direct numerical simulations and the ‘usual’ regularization model using linear filtering. Of the indicator functions studied, the best choice appears to be a synthesis of the Vreman and Q-criterion based indicator functions. When used by itself, the Q-criterion indicator is likely improvable with tuning/shifting so that laminar regions can be given less regularization.

REFERENCES

- [1] D.N. Arnold and J. Qin. Quadratic velocity/linear pressure Stokes elements. In R. Vichnevetsky, D. Knight, and G. Richter, editors, *Advances in Computer Methods for Partial Differential Equations VII*, pages 28–34. IMACS, 1992.
- [2] R. Betchov. Semi-isotropic turbulence and helicoidal flows. *Phys. Fluids*, 4:925–926, 1961.
- [3] A. Bowers and L. Rebholz. Increasing Accuracy and Efficiency in FE Computations of the Leray-Deconvolution Model. *Numerical Methods for Partial Differential Equations*, To appear, 2011.
- [4] S. Brenner and L.R. Scott. *The Mathematical Theory of Finite Element Methods*. Springer-Verlag, 1994.
- [5] M. Case, V. Ervin, A. Linke, and L. Rebholz. A connection between Scott-Vogelius and grad-div stabilized Taylor-Hood FE approximations of the Navier-Stokes equations. *SIAM Journal on Numerical Analysis*, 49(4):1461–1481, 2011.
- [6] A. Cheskidov, D. Holm, E. Olson, and E. Titi. On a Leray- α Model of Turbulence. *Proc Ser A Math Phys Eng Sci*, 461:629–649, 2005.
- [7] B. Cousins, L. Rebholz, and N. Wilson. Enforcing energy, helicity and strong mass conservation in FE computations for incompressible Navier-Stokes simulations. *Applied Mathematics and Computation*, To appear, 2010.

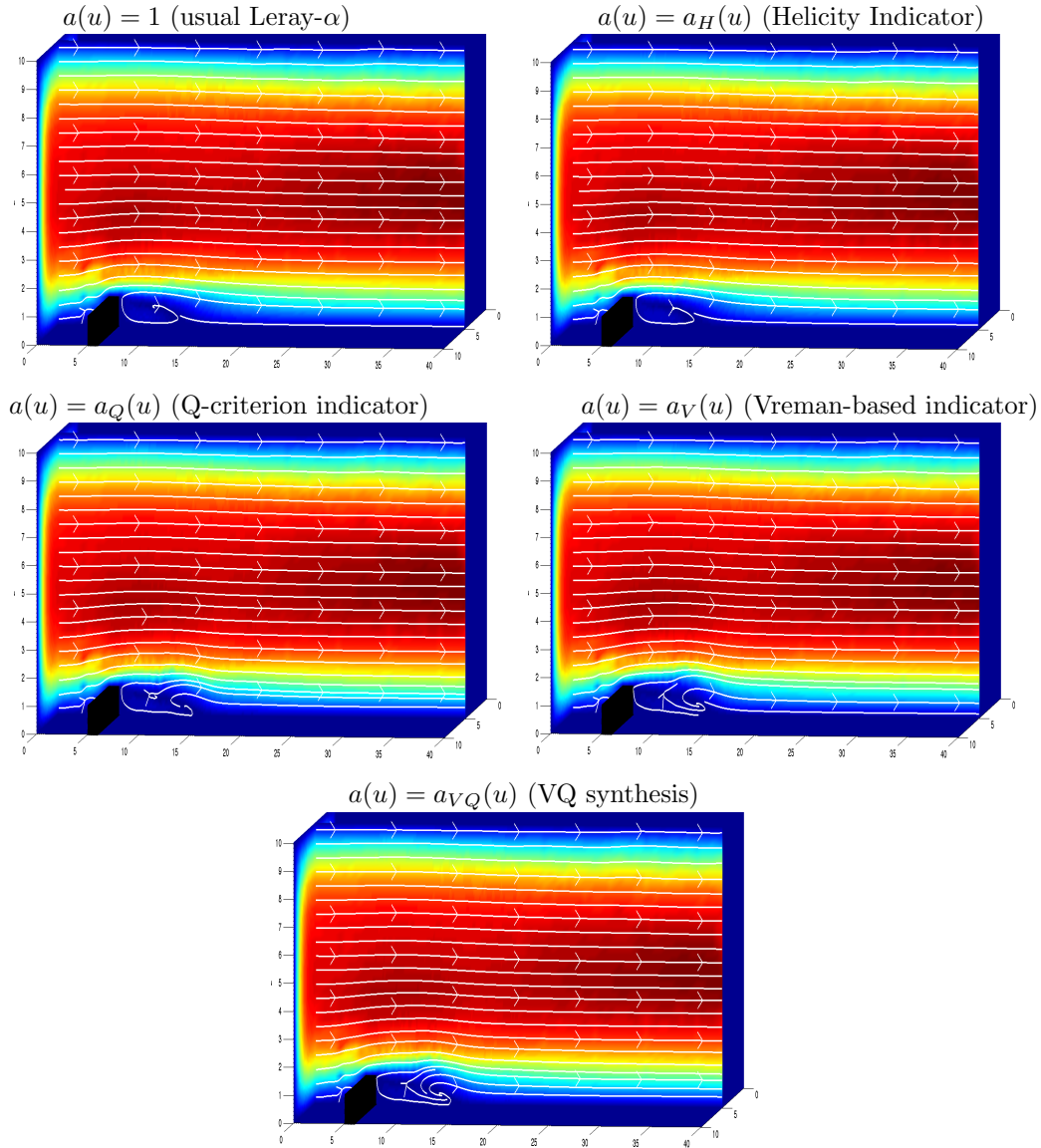


FIG. 3.10. Shown above is velocity streamlines and speed contours on the $x = 5$ sliceplanes of the $T = 10$ velocity solutions for 3D flow over a step, with several choices of indicator functions. The two plots involving the Vreman-based indicator function do the best job at resolving the eddy shedding and reformation.

- [8] E. Emmrich. Error of the two-step bdf for the incompressible navier-stokes problem. *M2AN*, 38(5):757–764, 2004.
- [9] G. Galdi and W. Layton. Approximating the larger eddies in fluid motion II: A model for space filtered flow. *Math. Methods and Models in Appl. Sci.*, 10(3):1–8, 2000.
- [10] B. J. Geurts and D. D. Holm. Regularization modeling for large eddy simulation. *Phys. Fluids*, 15:L13L16, 2003.
- [11] B. J. Geurts and D. D. Holm. Leray and lans-alpha modeling of turbulent mixing. *Journal of Turbulence*, 7:133, 2006.
- [12] M.D. Gunzburger. *Finite Element Methods for Viscous Incompressible Flows - A Guide to Theory, Practices, and Algorithms*. Academic Press, 1989.
- [13] A.A. Wray J.C. Hunt and P. Moin. Eddies stream and convergence zones in turbulent flows. *CTR report CTR-S88*, 1988.
- [14] V. John. Reference values for drag and lift of a two dimensional time-dependent flow around a cylinder. *International Journal for Numerical Methods in Fluids*, 44:777–788, 2004.
- [15] W. Layton. *Introduction to Finite Element Methods for Incompressible Viscous Flows*. SIAM, 2008.

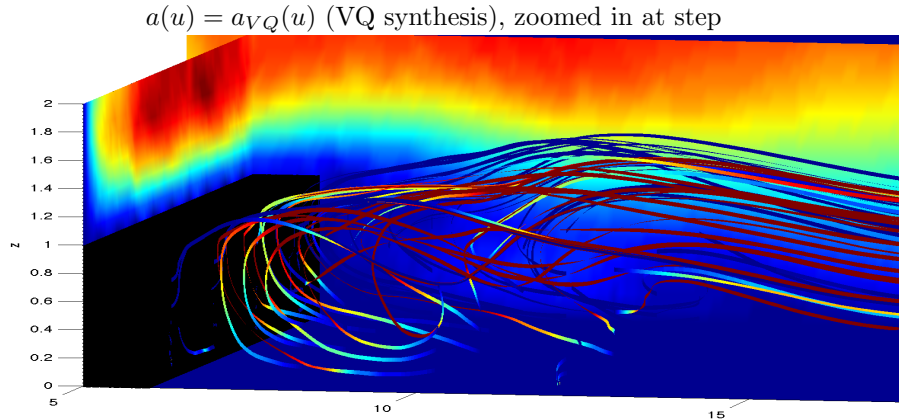


FIG. 3.11. Shown above is velocity streamribbons near the step for the $T = 10$ velocity solution for 3D flow over a step, obtained using the VQ indicator function. The eddy detachment and reformation is clear.

- [16] W. Layton, C. Manica, M. Neda, M.A. Olshanskii, and L. Rebholz. On the accuracy of the rotation form in simulations of the Navier-Stokes equations. *J. Comput. Phys.*, 228(5):3433–3447, 2009.
- [17] W. Layton, C. Manica, M. Neda, and L. Rebholz. Numerical Analysis and Computational Testing of a High Accuracy Leray-Deconvolution Model of Turbulence. *Numerical Methods for Partial Differential Equations*, 24(2):555–582, 2008.
- [18] W. Layton, C. Manica, M. Neda, and L. Rebholz. Numerical analysis and computational comparisons of the NS-omega and NS-alpha regularizations. *Comput. Methods Appl. Mech. Engrg.*, pages 916–931, 2009.
- [19] W. Layton, N. Mays, M. Neda, and C. Trenchea. Numerical analysis of modular regularization methods for the BDF2 time discretization of the Navier-Stokes equations. *Submitted*, 2011.
- [20] W. Layton, I. Stanculescu, and C. Trenchea. Theory of the NS- $\bar{\omega}$ model: a complement to the NS- α model. *Commun. Pure Appl. Anal.*, 10(6):1763–1777, 2011.
- [21] W. Layton, C. Trenchea, and L. Rebholz. Modular nonlinear filter stabilization of methods for higher Reynolds numbers flow. *Journal of Mathematical Fluid Mechanics*, To appear, 2011.
- [22] J. Leray. Essai sur le mouvement d’un fluide visqueux emplissant l’espace. *Acta. Math.*, 63:193–248, 1934.
- [23] E. Levich and A. Tsinober. Helical structures, fractal dimensions and renormalization group approach in homogeneous turbulence. *Physics Letters*, 96A:292–297, 1983.
- [24] E. Levich and A. Tsinober. On the role of helical structures in 3-dimensional turbulent flows. *Physics Letters*, 93A:293–297, 1983.
- [25] D.K. Lilly. The structure, energetics and propagation of rotating convection storms, II: Helicity and Storm Stabilization. *J. Atmos. Sciences*, 43:126–140, 1986.
- [26] M.A. Olshanskii and L. Rebholz. Application of barycenter refined meshes in linear elasticity and incompressible fluid dynamics. *Submitted*, 2011.
- [27] L. Rebholz. Conservation laws of turbulence models. *Journal of Mathematical Analysis and Applications*, 326(1):33–45, 2007.
- [28] L. Rebholz and M. Sussman. On the high accuracy NS- α -deconvolution model of turbulence. *Mathematical Models and Methods in Applied Sciences*, 20(4):611–633, 2010.
- [29] M. Schäfer and S. Turek. The benchmark problem ‘flow around a cylinder’ flow simulation with high performance computers II. in *E.H. Hirschel (Ed.), Notes on Numerical Fluid Mechanics*, 52, Braunschweig, Vieweg:547–566, 1996.
- [30] A. Tsinober and E. Levich. On the helical nature of 3-dimensional coherent structures in turbulent flows. *Physics Letters*, 99A:321–324, 1983.
- [31] M. van Reeuwijk, J. Jonker, and K. Hanjalic. Incompressibility of the Leray- α model for wall-bounded flows. *Physics of Fluids*, 18, 2006.
- [32] A.W. Vreman. An eddy-viscosity subgrid-scale model for turbulent shear flow: algebraic theory and applications. *Phys. Fluids*, 16:3670–3681, 2004.
- [33] S. Zhang. A new family of stable mixed finite elements for the 3d Stokes equations. *Mathematics of Computation*, 74:543–554, 2005.

5. Appendix.

Proof. [Proof of uniqueness of solutions of Algorithm 2.2]

Well-posedness of discrete solutions can be proven as follows. First, boundedness of velocity

solutions is already proven in , which gives us

$$\|u_h^M\|^2 + \nu \Delta t \sum_{n=0}^{M-1} \|\nabla u_h^{n+1/2}\|^2 \leq C(\text{data}).$$

Existence and uniqueness of discrete solutions can be reduced to existence and uniqueness at each timestep. Since the timestepping procedure linearizes the momentum equation and decouples the momentum/mass and filtering systems, the decoupled systems needing solved at each timestep take the form:

System 1: Solve the filter equation: Given u_h^n, u_h^{n-1} , find $U^{n+1} \in V_h$ satisfying

$$\alpha^2(a(\frac{3}{2}u_h^n - \frac{1}{2}u_h^{n-1})\nabla U^{n+1}, \nabla v_h) + (U^{n+1}, v_h) = (\frac{3}{2}u_h^n - \frac{1}{2}u_h^{n-1}, v_h) \quad \forall v_h \in V_h,$$

System 2: Given U_h^{n+1}, u_h^n find $u_h^{n+1} \in V_h$ satisfying

$$\frac{1}{\Delta t}(u_h^{n+1} - u_h^n, v_h) + b^*(U_h^{n+1}, u_h^{n+1/2}, v_h) + \nu(\nabla u_h^{n+1/2}, \nabla v_h) = (f^{n+1/2}, v_h) \quad (5.1)$$

Since each of these systems is linear and with number of equations equal to the number of unknowns, we need only prove uniqueness of solutions. For system 1, suppose two solutions, and let $e \in V_h$ denote their difference. Then

$$\alpha^2(a(\frac{3}{2}u_h^n - \frac{1}{2}u_h^{n-1})\nabla e, \nabla v_h) + (e, v_h) = 0 \quad \forall v_h \in V_h,$$

and letting $v_h = e$, we get

$$\int_{\Omega} a(\frac{3}{2}u_h^n - \frac{1}{2}u_h^{n-1})|\nabla e|^2 + \|e\|^2 = 0.$$

Since we require indicator functions to be bounded above 0, immediately we get $e=0$, and so solutions to System 1 must exist uniquely.

For System 2, again assume two solutions, u_1 and u_2 and let $e = u_1 - u_2$. Then we have

$$\frac{1}{\Delta t}(e, v_h) + b^*(U^{n+1}, e, v_h) + \nu(\nabla e, \nabla v_h) = 0 \quad \forall v_h \in V_h. \quad (5.2)$$

Now choosing $v_h = e$ gives

$$\frac{1}{\Delta t}\|e\|^2 + \nu\|\nabla e\|^2 = 0 \quad (5.3)$$

Thus, $e = 0$, and our solution is unique. Thus, from linearity and finite dimensionality, it exists uniquely. \square

Proof. [Proof of Theorem 2.7]

We begin with the velocity error. The smoothness required for the velocity convergence is $u \in L^\infty(0, T; H^{k+1}(\Omega)) \cap L^\infty(0, T; H^4(\Omega))$, $\nabla u_{tt} \in L^2(0, T; H^1(\Omega))$, and $u_{ttt} \in L^2(0, T; L^2(\Omega))$.

At time $t_{n+1/2}$, an NSE solution satisfies

$$\begin{aligned} & \left(\frac{u^{n+1} - u^n}{\Delta t}, v_h\right) + (\overline{E[u^n, u^{n-1}]}^h \cdot \nabla u^{n+1/2}, v_h) - (p^{n+1/2}, \nabla \cdot v_h) \\ & + \nu(\nabla u^{n+1/2}, \nabla v_h) = (f_{n+1/2}, v_h) + \text{Intp}(u^n, p^n; v_h) \end{aligned} \quad (5.4)$$

for all $v_h \in V_h$, where $\text{Intp}(u^n, p^n; v_h)$ denotes

$$\begin{aligned}
Intp(u^n, p^n; v_h) &= \left(\frac{u^{n+1} - u^n}{\Delta t} - u_t(t_{n+1/2}), v_h \right) + \overline{(E[u^n, u^{n-1}])^h} \cdot \nabla u^{n+1/2}, v_h \\
&\quad - (u(t_{n+1/2}) \cdot \nabla u(t_{n+1/2}), v_h) - (p_{n+1/2} - p(t_{n+1/2}), \nabla \cdot v_h) \\
&\quad + \nu (\nabla u^{n+1/2} - \nabla u(t_{n+1/2}), \nabla v_h) + (f(t_{n+1/2}) - f^{n+1/2}, v_h).
\end{aligned}$$

Then the error $e_n := u^n - u_h^n$ satisfies, for all $v_h \in V_h$,

$$\begin{aligned}
&\left(\frac{e_{n+1} - e_n}{\Delta t}, v_h \right) + \overline{(E[u^n, u^{n-1}])^h} \cdot \nabla u^{n+1/2}, v_h - \overline{(E[u_h^n, u_h^{n-1}])^h} \cdot \nabla u_h^{n+1/2}, v_h \\
&\quad - (p^{n+1/2} - p_h^{n+1/2}, \nabla \cdot v_h) + \nu (\nabla e_{n+1/2}, \nabla v_h) = Intp(u^n, p^n; v_h).
\end{aligned} \tag{5.5}$$

Since SV elements are being used, $v_h \in V_h$ implies $\nabla \cdot v_h = 0$, and so the pressure term vanishes. Next, decompose the error as $e_n = (u^n - U^n) - (u_h^n - U^n) := \eta^n - \phi_h^n$ where U^n is the L^2 projection of u^n into V_h , and $\phi_h^n \in V_h$. Setting $v_h = \phi_h^{n+1/2}$ in (5.5), we obtain

$$\begin{aligned}
\frac{1}{2\Delta t} (\|\phi_h^{n+1}\|^2 - \|\phi_h^n\|^2) + \nu \|\nabla \phi_h^{n+1/2}\|^2 &\leq \nu (\nabla \eta^{n+1/2}, \nabla \phi_h^{n+1/2}) - |Intp(u^n, p^n; \phi_h^{n+1/2})| \\
&\quad + \overline{(E[u^n, u^{n-1}])^h} \cdot \nabla u^{n+1/2}, \phi_h^{n+1/2} - \overline{(E[u_h^n, u_h^{n-1}])^h} \cdot \nabla u_h^{n+1/2}, \phi_h^{n+1/2}.
\end{aligned} \tag{5.6}$$

We now bound the terms in the RHS of (5.6) individually. Cauchy-Schwarz and Young's inequalities give

$$\begin{aligned}
\nu (\nabla \eta^{n+1/2}, \nabla \phi_h^{n+1/2}) &\leq \nu \|\nabla \eta^{n+1/2}\| \|\nabla \phi_h^{n+1/2}\| \\
&\leq \varepsilon \nu \|\nabla \phi_h^{n+1/2}\|^2 + C \nu \|\nabla \eta^{n+1/2}\|^2.
\end{aligned} \tag{5.7}$$

In order to bound the nonlinear terms we will need the following lemmas.

DEFINITION 5.1. *Assume that X_h, Q_h satisfy the discrete inf-sup condition. Given an indicator function $a(\cdot)$, $w_h \in V_h$, and $w \in X$ we define the frozen nonlinearity filtered velocity \widehat{w}_h using the selected indicator function as the solution of:*

$$\alpha^2 (a(w_h) \nabla \widehat{w}_h, \nabla \chi_h) + (\widehat{w}_h, \chi_h) = (w, \chi_h) \quad \forall \chi_h \in V_h. \tag{5.8}$$

Now we consider the error in $\widehat{w}_h - \overline{w}_h^h$.

LEMMA 5.2. *Let X_h, Q_h satisfy the discrete inf-sup condition. We have*

$$\alpha^2 \int_{\Omega} a(w_h) |\nabla (\widehat{w}_h - \overline{w}_h^h)|^2 + \frac{\|\widehat{w}_h - \overline{w}_h^h\|^2}{2} \leq \frac{\|w - w_h\|^2}{2}.$$

Proof. By definition of \overline{w}_h^h

$$\alpha^2 (a(w_h) \nabla \overline{w}_h^h, \nabla \chi_h) + (\overline{w}_h^h, \chi_h) = (w_h, \chi_h) \quad \forall \chi_h \in V_h. \tag{5.9}$$

Subtracting (5.9) from (5.8) and choosing $\chi_h = \widehat{w}_h - \overline{w}_h^h$ we obtain

$$\alpha^2 \int_{\Omega} a(w_h) |\nabla (\widehat{w}_h - \overline{w}_h^h)|^2 + \|\widehat{w}_h - \overline{w}_h^h\|^2 = (w - w_h, \widehat{w}_h - \overline{w}_h^h).$$

Young's inequality completes the proof. \square

LEMMA 5.3. *Let X_h, Q_h satisfy the discrete inf-sup condition. We have*

$$\begin{aligned}
\|\overline{w}^h - \overline{w}_h^h\|^2 &\leq C (\|w - w_h\|^2 + \alpha^2 \min\{\|\nabla w\|^2, \alpha^2 \|\nabla \cdot (a(w_h) \nabla w)\|^2\}) \\
&\quad + \inf_{\chi \in V_h} \{\alpha^2 \|\nabla (w - \chi)\|^2 + \|w - \chi\|^2\} + \alpha^4 \|\nabla \cdot (a(w) \nabla w)\|^2.
\end{aligned} \tag{5.10}$$

Proof. Let us rewrite $\bar{w}^h - \bar{w}_h^h$ as $(\bar{w}^h - w) + (\widehat{w}_h - \bar{w}_h^h) + (w - \widehat{w}_h)$. Applying the triangle inequality along with the previous lemma, Theorem 2.1 and Lemma A.2 in [21] finishes the proof. \square

For the nonlinear terms, we first write them as

$$\begin{aligned}
& (\overline{E[u^n, u^{n-1}]^h} \cdot \nabla u^{n+1/2}, \phi_h^{n+1/2}) - (\overline{E[u_h^n, u_h^{n-1}]^h} \cdot \nabla u_h^{n+1/2}, \phi_h^{n+1/2}) \\
&= ((\overline{E[u^n, u^{n-1}]^h} - \overline{E[u_h^n, u_h^{n-1}]^h}) \cdot \nabla u^{n+1/2}, \phi_h^{n+1/2}) + (\overline{E[u_h^n, u_h^{n-1}]^h} \cdot \nabla e_{n+1/2}, \phi_h^{n+1/2}) \\
&= ((\overline{E[u^n, u^{n-1}]^h} - \overline{E[u_h^n, u_h^{n-1}]^h}) \cdot \nabla u^{n+1/2}, \phi_h^{n+1/2}) + (\overline{E[u_h^n, u_h^{n-1}]^h} \cdot \nabla \eta^{n+1/2}, \phi_h^{n+1/2}) \\
&= ((\overline{E[u^n, u^{n-1}]^h} - \overline{E[u_h^n, u_h^{n-1}]^h}) \cdot \nabla u^{n+1/2}, \phi_h^{n+1/2}) + (\overline{E[u^n, u^{n-1}]^h} \cdot \nabla \eta^{n+1/2}, \phi_h^{n+1/2}) \\
&\quad - ((\overline{E[u^n, u^{n-1}]^h} - \overline{E[u_h^n, u_h^{n-1}]^h}) \cdot \nabla \eta^{n+1/2}, \phi_h^{n+1/2}), \tag{5.11}
\end{aligned}$$

and bound them separately:

$$|(\overline{E[u^n, u^{n-1}]^h} \cdot \nabla \eta^{n+1/2}, \phi_h^{n+1/2})| \leq \varepsilon \nu \|\nabla \phi_h^{n+1/2}\|^2 + C \|\nabla \eta^{n+1/2}\|^2. \tag{5.12}$$

From (5.10) we have

$$\begin{aligned}
& |((\overline{E[u^n, u^{n-1}]^h} - \overline{E[u_h^n, u_h^{n-1}]^h}) \cdot \nabla u^{n+1/2}, \phi_h^{n+1/2})| \\
&\leq C \|(\overline{E[u^n, u^{n-1}]^h} - \overline{E[u_h^n, u_h^{n-1}]^h})\| \|\nabla u^{n+1/2}\|_{L^\infty(\Omega)} \|\nabla \phi_h^{n+1/2}\| \\
&\leq \varepsilon \nu \|\nabla \phi_h^{n+1/2}\|^2 + C \left(\|E[e_n, e_{n-1}]\|^2 + \alpha^4 + (\alpha^2 h^{2k} + h^{2k+2}) \|u\|_{L^\infty(0, T; H^{k+1}(\Omega))}^2 \right) \\
&\leq \varepsilon \nu \|\nabla \phi_h^{n+1/2}\|^2 + C \left(\|E[\eta^n, \eta^{n-1}]\|^2 + \|E[\phi_h^n, \phi_h^{n-1}]\|^2 + \alpha^4 + h^{2k} \right) \\
&\leq \varepsilon \nu \|\nabla \phi_h^{n+1/2}\|^2 + C \left(\|\eta^n\|^2 + \|\eta^{n-1}\|^2 + \alpha^4 + h^{2k} \right) + C \left(\|\phi_h^n\|^2 + \|\phi_h^{n-1}\|^2 \right). \tag{5.13}
\end{aligned}$$

Using the assumption that the mesh is quasi-uniform, by the inverse inequality we have

$$\begin{aligned}
& |((\overline{E[u^n, u^{n-1}]^h} - \overline{E[u_h^n, u_h^{n-1}]^h}) \cdot \nabla \eta^{n+1/2}, \phi_h^{n+1/2})| \\
&\leq \varepsilon \nu \|\nabla \phi_h^{n+1/2}\|^2 + Ch^{-1} \|(\overline{E[u^n, u^{n-1}]^h} - \overline{E[u_h^n, u_h^{n-1}]^h})\|^2 \|\nabla \eta^{n+1/2}\|^2 \\
&\leq \varepsilon \nu \|\nabla \phi_h^{n+1/2}\|^2 + Ch^{-1} \left(\|E[\eta^n, \eta^{n-1}]\|^2 + \|E[\phi_h^n, \phi_h^{n-1}]\|^2 + \alpha^4 + \alpha^2 h^{2k} + h^{2k+2} \right) \|\nabla \eta^{n+1/2}\|^2 \\
&\leq \varepsilon \nu \|\nabla \phi_h^{n+1/2}\|^2 + Ch^{-1} \left(h^{2k+2} \|u\|_{L^\infty(0, T; H^{k+1}(\Omega))}^2 + \|\phi_h^n\|^2 + \|\phi_h^{n-1}\|^2 + \alpha^4 + \alpha^2 h^{2k} \right) \|\nabla \eta^{n+1/2}\|^2. \tag{5.14}
\end{aligned}$$

Combining (5.6)-(5.7), (5.11)-(5.14) and summing from $n = 0$ to $M - 1$ (assuming that $\|\phi_h^0\| = 0$) we obtain

$$\begin{aligned}
& \|\phi_h^M\|^2 + \nu \frac{\Delta t}{2} \sum_{n=0}^{M-1} \|\nabla \phi_h^{n+1/2}\|^2 \\
&\leq C(1 + h^{2k-1} + h^{-1} \alpha^4) \sum_{n=0}^M \Delta t \|\nabla \eta^n\|^2 + C \Delta t \sum_{n=0}^{M-1} \|\phi_h^n\|^2 (1 + h^{-1} \|\nabla \eta^{n+1/2}\|^2) \\
&\quad + \sum_{n=0}^{M-1} \Delta t |Intp(u^n, p^n; \phi_h^{n+1/2})| + CT(\alpha^4 + h^{2k}). \tag{5.15}
\end{aligned}$$

Let us introduce the following discrete norm:

$$\|u\|_{m,k} := \left(\Delta t \sum_{n=0}^{N_T} \|u(t_n)\|_k^m \right)^{1/m}.$$

We continue to bound the terms on the right-hand side of (5.15):

$$C \sum_{n=0}^M \Delta t \|\nabla \eta^n\|^2 \leq C \Delta t \sum_{n=0}^M h^{2k} |u^n|_{k+1}^2 \leq C h^{2k} \|u\|_{2,k+1}^2 \quad (5.16)$$

$$\begin{aligned} C \Delta t \sum_{n=0}^{M-1} \|\phi_h^n\|^2 (1 + h^{-1} \|\nabla \eta^{n+1/2}\|^2) &\leq C \Delta t \sum_{n=0}^{M-1} \|\phi_h^n\|^2 (1 + h^{2k-1} \|u\|_{L^\infty(0,T;H^{k+1}(\Omega))}^2) \\ &\leq C \Delta t \sum_{n=0}^{M-1} \|\phi_h^n\|^2. \end{aligned} \quad (5.17)$$

We now bound the terms in $\text{Intp}(u^n; p^n; \phi_h^{n+1/2})$. Using the standard inequalities and the error estimate for the discrete filter,

$$\begin{aligned} &(\overline{E[u^n, u^{n-1}]^h} \cdot \nabla u^{n+1/2}, \phi_h^{n+1/2}) - (u(t_{n+1/2}) \cdot \nabla u(t_{n+1/2}), \phi_h^{n+1/2}) \\ &= ((\overline{E[u^n, u^{n-1}]^h} - E[u^n, u^{n-1}]) \cdot \nabla u^{n+1/2}, \phi_h^{n+1/2}) + ((E[u^n, u^{n-1}] - u(t_{n+1/2})) \cdot \nabla u^{n+1/2}, \phi_h^{n+1/2}) \\ &\quad + (u(t_{n+1/2}) \cdot \nabla (u^{n+1/2} - u(t_{n+1/2})), \phi_h^{n+1/2}) \\ &\leq 3\varepsilon \|\nabla \phi_h^{n+1/2}\|^2 + C(\alpha^2 h^{2k} + h^{2k+2}) |E[u^n, u^{n-1}]|_{k+1}^2 + C\alpha^4 \|\nabla \cdot (a(E[u^n, u^{n-1}]) \nabla E[u^n, u^{n-1}])\|^2 \\ &\quad + C(\Delta t)^4 \|\nabla u_{tt}\|^2 + C(\Delta t)^3 \int_{t_n}^{t_{n+1}} \|\nabla u_{tt}\|^2 dt. \end{aligned} \quad (5.18)$$

Combine (5.18) and [15] to obtain

$$\begin{aligned} &\Delta t \sum_{n=0}^{M-1} |\text{Intp}(u^n, p^n; \phi_h^{n+1/2})| \\ &\leq 7\varepsilon \Delta t \sum_{n=0}^{M-1} \|\nabla \phi_h^{n+1/2}\|^2 + C(\Delta t)^4 (\|u_{ttt}\|_{2,0}^2 + \|f_{tt}\|_{2,0}^2 + \|\nabla u_{tt}\|_{2,0}^2) \\ &\quad + C(\alpha^2 h^{2k} + h^{2k+2}) \|u\|_{0,k+1}^2 + C\alpha^4 \|\nabla \cdot (a(E[u^n, u^{n-1}]) \nabla E[u^n, u^{n-1}])\|_{2,0}^2. \end{aligned} \quad (5.19)$$

Putting everything together we get

$$\begin{aligned} &\|\phi_h^M\|^2 + \nu \frac{\Delta t}{4} \sum_{n=0}^{M-1} \|\nabla \phi_h^{n+1/2}\|^2 \\ &\leq C \Delta t \sum_{n=0}^{M-1} \|\phi_h^n\|^2 + C h^{2k} \|u\|_{2,k+1}^2 + C\alpha^4 (\|\nabla \cdot (a(E[u^n, u^{n-1}]) \nabla E[u^n, u^{n-1}])\|_{2,0}^2 + \|u\|_{L^\infty(0,T;H^{k+1}(\Omega))}^2) \\ &\quad + C(\Delta t)^4 (\|u_{ttt}\|_{2,0}^2 + \|f_{tt}\|_{2,0}^2 + \|\nabla u_{tt}\|_{2,0}^2) + C(\alpha^2 h^{2k} + h^{2k+2}) \|u\|_{0,k+1}^2. \end{aligned} \quad (5.20)$$

Applying Gronwall's lemma along with the triangle inequality gives us (2.11). In order to prove (2.12) we will additionally assume that

$$\Delta u_{tt} \in L^2(0, T; L^2(\Omega)).$$

We will now derive a bound that will be used in proving the (2.12). Let us again consider (5.5). Decompose the velocity error as $e_n = (u^n - U^n) - (u_h^n - U^n) := \eta^n - \phi_h^n$ where $\phi_h^n \in V^h$, and U^n is the Stokes projection of u^n in V^h . Setting $v_h = \frac{\phi_h^{n+1} - \phi_h^n}{\Delta t} \in V^h$ in (5.5) we obtain that

$$\begin{aligned}
& \left\| \frac{\phi_h^{n+1} - \phi_h^n}{\Delta t} \right\|^2 + \nu \frac{\|\nabla \phi_h^{n+1}\|^2 - \|\nabla \phi_h^n\|^2}{2\Delta t} \\
&= \left(\frac{\eta^{n+1} - \eta^n}{\Delta t}, \frac{\phi_h^{n+1} - \phi_h^n}{\Delta t} \right) + \nu \left(\nabla \frac{\eta^{n+1} + \eta^n}{2}, \nabla \frac{\phi_h^{n+1} - \phi_h^n}{\Delta t} \right) \\
&\quad - \left(\frac{p(t_{n+1}) + p(t_n)}{2} - q^h, \nabla \cdot \frac{\phi_h^{n+1} - \phi_h^n}{\Delta t} \right) \\
&\quad + \left((\overline{E[u^n, u^{n-1}]^h} - \overline{E[u_h^n, u_h^{n-1}]^h}) \cdot \nabla u^{n+1/2}, \frac{\phi_h^{n+1} - \phi_h^n}{\Delta t} \right) \\
&\quad - \left((\overline{E[u^n, u^{n-1}]^h} - \overline{E[u_h^n, u_h^{n-1}]^h}) \cdot \nabla e_{n+1/2}, \frac{\phi_h^{n+1} - \phi_h^n}{\Delta t} \right) \\
&\quad + \left(\overline{E[u^n, u^{n-1}]^h} \cdot \nabla e_{n+1/2}, \frac{\phi_h^{n+1} - \phi_h^n}{\Delta t} \right) \\
&\quad + \text{Intp}(u, p; \frac{\phi_h^{n+1} - \phi_h^n}{\Delta t}), \tag{5.21}
\end{aligned}$$

where, using Taylor expansion

$$\begin{aligned}
& \text{Intp}(u, p; \frac{\phi_h^{n+1} - \phi_h^n}{\Delta t}) \\
&= \left(\frac{u^{n+1} - u^n}{\Delta t} - u_t(t_{n+1/2}), \frac{\phi_h^{n+1} - \phi_h^n}{\Delta t} \right) + \left(\overline{E[u^n, u^{n-1}]^h} \cdot \nabla u^{n+1/2}, \frac{\phi_h^{n+1} - \phi_h^n}{\Delta t} \right) \\
&\quad - \left(u(t_{n+1/2}) \cdot \nabla u(t_{n+1/2}), \frac{\phi_h^{n+1} - \phi_h^n}{\Delta t} \right) + \nu \left(\nabla u^{n+1/2} - \nabla u(t_{n+1/2}), \nabla \frac{\phi_h^{n+1} - \phi_h^n}{\Delta t} \right) \\
&\quad + \left(f(t_{n+1/2}) - f^{n+1/2}, \frac{\phi_h^{n+1} - \phi_h^n}{\Delta t} \right). \tag{5.22}
\end{aligned}$$

It follows from the definition of the Stokes projection that

$$\nu \left(\nabla \frac{\eta^{n+1} + \eta^n}{2}, \nabla \frac{\phi_h^{n+1} - \phi_h^n}{\Delta t} \right) - \left(\frac{p(t_{n+1}) + p(t_n)}{2} - q^h, \nabla \cdot \frac{\phi_h^{n+1} - \phi_h^n}{\Delta t} \right) = 0. \tag{5.23}$$

We now bound the three nonlinear terms on the right-hand side of (5.21). For the first term use the generalized Holder's inequality

$$\begin{aligned}
& \left((\overline{E[u^n, u^{n-1}]^h} - \overline{E[u_h^n, u_h^{n-1}]^h}) \cdot \nabla u^{n+1/2}, \frac{\phi_h^{n+1} - \phi_h^n}{\Delta t} \right) \\
&\leq \| (\overline{E[u^n, u^{n-1}]^h} - \overline{E[u_h^n, u_h^{n-1}]^h}) \| \| \nabla u^{n+1/2} \|_{L^\infty(\Omega)} \| \frac{\phi_h^{n+1} - \phi_h^n}{\Delta t} \| \\
&\leq \varepsilon \| \frac{\phi_h^{n+1} - \phi_h^n}{\Delta t} \|^2 + C \| (\overline{E[u^n, u^{n-1}]^h} - \overline{E[u_h^n, u_h^{n-1}]^h}) \|^2 \\
&\leq \varepsilon \| \frac{\phi_h^{n+1} - \phi_h^n}{\Delta t} \|^2 + C (\|E[e_n, e_{n-1}]\|^2 + \alpha^4 + h^{2k}) \\
&\leq \varepsilon \| \frac{\phi_h^{n+1} - \phi_h^n}{\Delta t} \|^2 + C(\Delta t^4 + h^{2k} + \alpha^4). \tag{5.24}
\end{aligned}$$

For the second term use the bound for the nonlinear terms, error estimate for the discrete

filter, inverse and Young's inequalities to get

$$\begin{aligned}
& ((\overline{E[u^n, u^{n-1}]^h} - \overline{E[u_h^n, u_h^{n-1}]^h}) \cdot \nabla e_{n+1/2}, \frac{\phi_h^{n+1} - \phi_h^n}{\Delta t}) \\
& \leq Ch^{-3/2} \|(\overline{E[u^n, u^{n-1}]^h} - \overline{E[u_h^n, u_h^{n-1}]^h})\| \|\nabla e_{n+1/2}\| \|\frac{\phi_h^{n+1} - \phi_h^n}{\Delta t}\| \\
& \leq \varepsilon \|\frac{\phi_h^{n+1} - \phi_h^n}{\Delta t}\|^2 + Ch^{-3} \|\nabla e_{n+1/2}\|^2 (h^{2k} + (\Delta t)^4 + \alpha^4).
\end{aligned} \tag{5.25}$$

For the third term use the inverse and Young's inequalities to get

$$\begin{aligned}
& (\overline{E[u^n, u^{n-1}]^h} \cdot \nabla e_{n+1/2}, \frac{\phi_h^{n+1} - \phi_h^n}{\Delta t}) \\
& \leq Ch^{-1/2} \|\nabla \overline{E[u^n, u^{n-1}]^h}\| \|\nabla e_{n+1/2}\| \|\frac{\phi_h^{n+1} - \phi_h^n}{\Delta t}\| \\
& \leq \varepsilon \|\frac{\phi_h^{n+1} - \phi_h^n}{\Delta t}\|^2 + Ch^{-1} \|\nabla e_{n+1/2}\|^2.
\end{aligned} \tag{5.26}$$

As in (5.18), we obtain that

$$\begin{aligned}
& |Intp(u, p; \frac{\phi_h^{n+1} - \phi_h^n}{\Delta t})| \\
& \leq 5\varepsilon \|\frac{\phi_h^{n+1} - \phi_h^n}{\Delta t}\|^2 + \|(\frac{u^{n+1} - u^n}{\Delta t} - u_t(t_{n+1/2}))\|^2 + \|(f(t_{n+1/2}) - f^{n+1/2})\|^2 \\
& + \|\overline{E[u^n, u^{n-1}]^h} \cdot \nabla u^{n+1/2} - u(t_{n+1/2}) \cdot \nabla u(t_{n+1/2})\|^2 \\
& + C\nu(\Delta t)^3 \|\Delta u_{tt}\|_{L^2(t_n, t_{n+1}; L^2(\Omega))}^2.
\end{aligned} \tag{5.27}$$

Inserting the bounds (5.24)-(5.27) into (5.22), multiplying by $2\Delta t$ and summing from 0 to $M-1$ we get

$$\begin{aligned}
& 2\Delta t \sum_{n=0}^{M-1} \|\frac{\phi_h^{n+1} - \phi_h^n}{\Delta t}\|^2 + \nu \|\nabla \phi_h^M\|^2 \\
& \leq C((\Delta t)^4 + \alpha^4 + h^{2k}) + Ch^{2k+2} \|u_t\|_{L^2(0, T; H^{m+1}(\Omega))}^2 \\
& + C(h^{-1} + h^{-3}((\Delta t)^4 + \alpha^4 + h^{2k})) \Delta t \sum_{n=0}^{M-1} \|\nabla e_{n+1/2}\|^2.
\end{aligned} \tag{5.28}$$

Applying (2.11) and the triangle inequality gives

$$\begin{aligned}
& \Delta t \sum_{n=0}^{M-1} \|\frac{e_{n+1} - e_n}{\Delta t}\|^2 + \nu \|\nabla e_M\|^2 \\
& \leq C(h^{-1}((\Delta t)^4 + \alpha^4 + h^{2k}) + h^{-3}((\Delta t)^8 + \alpha^8 + h^{4k})).
\end{aligned} \tag{5.29}$$

Now we prove (2.12). For any $v_h \in X^h$ we have

$$\begin{aligned}
& (u_t(t_{n+1/2}) - \frac{u_h^{n+1} - u_h^n}{\Delta t}, v_h) + (u(t_{n+1/2}) \cdot \nabla u(t_{n+1/2}) \\
& - \overline{E[u_h^n, u_h^{n-1}]^h} \cdot \nabla u_h^{n+1/2}, v_h) - (p(t_{n+1/2}) - p_h^{n+1/2}, \nabla \cdot v_h) \\
& + \nu(\nabla u(t_{n+1/2}) - \nabla u_h^{n+1/2}, \nabla v_h) = 0.
\end{aligned} \tag{5.30}$$

Decompose the pressure approximation error into

$$p(t_{n+1}) - p_h^{n+1} = (p(t_{n+1}) - I(p)) - (p_h^{n+1} - I(p)) = q^{n+1} - r_h^{n+1}, \quad (5.31)$$

where $r_h^{n+1} \in Q^h$, $I(p)$ is a projection of $p(t_{n+1})$ into Q^h . Using the error decomposition (5.31) in (5.30) and applying the discrete LBB^h condition we obtain

$$\begin{aligned} \beta^h \|r_h^{n+1/2}\| &\leq C \left(\|u_t(t_{n+1/2}) - \frac{u(t_{n+1}) - u(t_n)}{\Delta t}\| + \left\| \frac{e_{n+1} - e_n}{\Delta t} \right\| \right) \\ &+ C \| (p(t_{n+1/2}) - I(p)) \| + \|\nabla(u(t_{n+1/2}) - u^{n+1/2})\| + \|\nabla e_{n+1/2}\| + \|u(t_{n+1/2})\nabla e_{n+1/2}\| \\ &+ \|(u(t_{n+1/2}) - E[u^n, u^{n-1}])\nabla u_h^{n+1/2}\| + \|(\overline{E[u^n, u^{n-1}]}^h - E[u^n, u^{n-1}])\nabla u_h^{n+1/2}\|. \end{aligned} \quad (5.32)$$

Taylor expansion and stability of u_h^n gives

$$\begin{aligned} \beta^h \|r_h^{n+1/2}\| &\leq C((\Delta t)^2 + \alpha h^k + h^{k+1}) + h^s \|p\|_{H^s(\Omega)} \\ &+ \left\| \frac{e_{n+1} - e_n}{\Delta t} \right\| + \|\nabla e_{n+1/2}\|. \end{aligned} \quad (5.33)$$

Squaring both sides of (5.33), sum from 0 to $M-1$ and multiply by Δt gives

$$\begin{aligned} \Delta t \sum_{n=0}^{M-1} \|r_h^{n+1/2}\|^2 &\leq C(u, T, \nu)((\Delta t)^4 + \alpha^2 h^{2k} + h^{\min\{2k+2, 2s\}}) \\ &+ \Delta t \sum_{n=0}^{M-1} \left(\left\| \frac{e_{n+1} - e_n}{\Delta t} \right\|^2 + \|\nabla e_{n+1/2}\|^2 \right). \end{aligned} \quad (5.34)$$

Applying (5.29) yields

$$\begin{aligned} \Delta t \sum_{n=0}^{M-1} \|r_h^{n+1/2}\|^2 &\leq C(u, T, \nu)((\Delta t)^4 + \alpha^2 h^{2k} + h^{\min\{2k+2, 2s\}}) \\ &+ C(h^{-1}((\Delta t)^4 + \alpha^4 + h^{2k}) + h^{-3}((\Delta t)^8 + \alpha^8 + h^{4k})). \end{aligned} \quad (5.35)$$

The triangle inequality finishes the proof. \square